Formation of Hexagonal Boron Nitride by Metal Atomic Vacancy-Assisted B—N Molecular Diffusion

Seongjun Park,[†,∥] Jinyeong Lee,[§,∥] Han Sol Kim,[§] Jong-Bong Park,[‡] Kang Hyuck Lee,[§] Sang A Han,[§] Sungwoo Hwang,[†] Sang-Woo Kim,[*,§] and Hyeon-Jin Shin[*,†]

[†]Nano electronics Laboratory and [‡]Platform Technology Laboratory, Samsung Advanced Institute of Technology, Suwon 443-801, Republic of Korea and [§]School of Advanced Materials Science and Engineering, SKKU Advanced Institute of Nanotechnology (SAINT), Sungkyunkwan University (SKKU), Suwon 440-746, Republic of Korea. [∥]These authors contributed equally to this work.

ABSTRACT Because of the low solubility of N atoms in metals, hexagonal boron nitride (h-BN) growth has explained by surface reaction on metal rather than by penetration/precipitation of B and N atoms in metal. Here, we present an impressive pathway of h-BN formation at the interface between Ni and oxide substrate based on B—N molecular diffusion into Ni through individual atomic vacancies. First-principles calculations confirmed the formation energies of the h-BN layers on and under the metal and the probability of B—N molecular diffusion in metal. The interface growth behavior depends on the species of metal catalysts, and these simulation results well support experimental results.

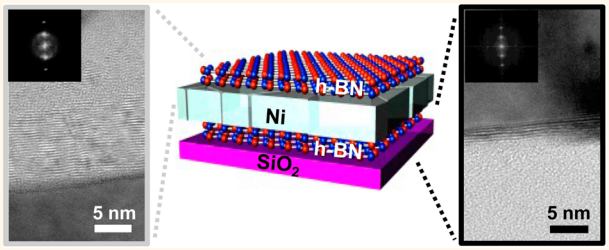

KEYWORDS: hexagonal boron nitride · B—N molecular diffusion · growth mechanism · interfacial growth

Since the discovery of graphene, its device application has been continuously considered. In particular, to overcome the limitation of improvements to performance and capacity through dimensional scale in silicon-based electronics, attention in this field has turned to graphene electronics.[1] However, a new concept device structure was needed due to the poor on/off ratio resulting from graphene's zero-band gap. A graphene barrier transistor with an interface between graphene and silicon[2] and/or vertically stacked graphene devices with two-dimensional (2D) layered material, h-BN,[3] molybdenum disulfide (MoS_2),[4] and tungsten disulfide (WS_2)[5] was introduced and demonstrated improvement of the on/off ratio and current density by modulation of Schottky or tunneling barrier height at the material interface. In those structures, 2D-layered materials are key components for high performance. However, it still used mechanically exfoliated material, and the growth behavior for large size electronics is not yet clearly understood.

Understanding the growth behavior of 2D-layered materials, from conducting graphene[6,7] and semiconducting MoS_2[8] to insulating h-BN,[9−11] use of chemical vapor deposition (CVD) is crucial to achieving quality-controlled 2D layered materials with the promising properties of large-area scalability, high crystallinity, low defect density, *etc*. In a typical CVD process, the surface reaction and surface diffusion of the precursor are two critical factors affecting layer deposition.[12] To overcome the surface reaction barrier and induce multiple chemical transformations, metal substrates are often used for the synthesis of 2D-layered materials.

The formation of graphene can be explained by two mechanisms: (i) a surface reaction by competitive adsorption and desorption on metal[7] and (ii) carbon segregation from a metal with significant carbon solubility.[6,13] Because of the low solubility of N atoms in metal,[14,15] the formation of h-BN, which has a structure similar to that of graphene, has been explained mainly as a surface reaction on metal involving the polymerization and recrystallization of BN precursors.[10,16] Recently, the formation of h-BN on both the top and bottom surfaces of the metal film has been reported, and its growth

* Address correspondence to kimsw1@skku.edu, hyeonjin.shin@samsung.com.

Received for review October 19, 2014 and accepted December 8, 2014.

Published online December 08, 2014
10.1021/nn505960b

mechanism has been presumed by mass transport through the metal film.[17,18] Although formation of the h-BN layer has been observed by experiment, growth mechanisms have not been understood clearly.

Here, we report an impressive pathway for h-BN layer formation based on B−N molecular diffusion through individual atomic vacancies in the metal. Until now, it was believed that molecular diffusion in metal was difficult to achieve. Nevertheless, by this method, h-BN layers could be grown at the interface between Ni and an underlying oxide substrate with a clean surface, which could be attractive for 2D electronics. To investigate the mechanism of h-BN formation, the formation energies of the h-BN layers and the reaction energies of the BN precursors both on and under the surfaces of Ni and Cu were determined using first-principles calculations based on density function theory (DFT).[19] It was found that h-BN growth behavior at the interface is distinctly different for Ni and Cu, which was in good agreement with the experimental results. Furthermore, to further clarify the role of B−N molecular diffusion on the formation of h-BN at the Ni/SiO_2 interface, h-BN formation was investigated using a solid precursor at varying concentrations.

RESULTS AND DISCUSSION

h-BN layers were synthesized on polycrystalline Ni thin films (300 nm thickness) deposited on SiO_2/Si substrates. The h-BN layer formation was achieved in an ambient pressure CVD system using an ammonia borane (AB, $H_3B{-}NH_3$) source, as previously described.[10] Figure 1a shows a transmission electron microscopy (TEM) image of h-BN layers. Importantly, high-resolution (HR) TEM images show that crystalline h-BN layers were grown not only on top of the Ni surface (Figure 1b) but also at the interface between Ni and the underlying oxide (Figure 1c). The fast Fourier transform (FFT) pattern of both the top and interfacial layers indicated the typical hexagonal structure of h-BN with (0002) lattices. The interlayer distance was approximately 3.4 Å, which is equal to the van der Waals interaction distance.[20]

To better define the structure of the two layers, we carried out electron energy loss spectroscopy (EELS) measurements (Figure 1d). Both layers consisted of visible edges starting at 191 and 400 eV, which correspond to the characteristic *K*-shell ionization edges of B and N, respectively.[21,22] The *K*-edge absorptions of B and N atoms exhibited sharp peaks followed by wider bands, which correspond to the 1s−π* and 1s−σ* transitions, respectively. These data provide clear evidence of sp^2-hybridization, indicating the hexagonal arrangement of B and N atoms in each layer. Furthermore, elemental analysis by energy-filtered TEM (EF-TEM) and depth profiling by X-ray photoelectron spectroscopy (XPS) clearly showed that B and N atoms were not present in the Ni (see the Supporting Information,

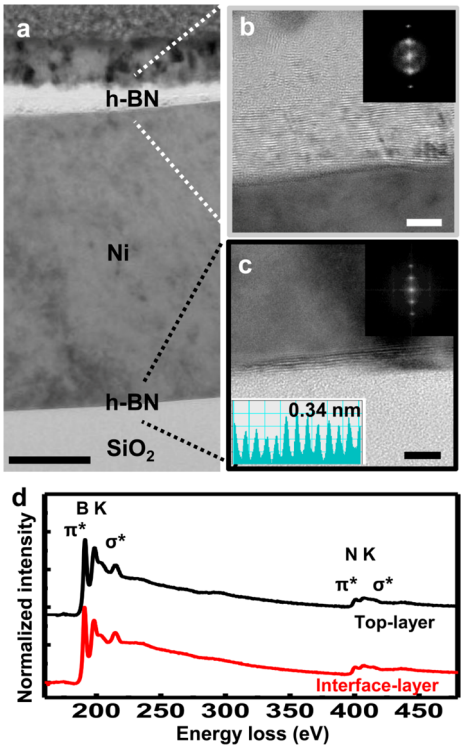

Figure 1. Characterization of CVD grown h-BN layers using an AB precursor. (a) TEM image of h-BN layers. HR-TEM images. (b) On top of the Ni surface (c) At interface between Ni and SiO_2/Si substrate. FFT patterns of both the top and interfacial layers and interlayer distance were shown in inset image. Scales bars, 100 nm (left) and 5 nm (right). (d) EELS of the both layers.

Figure S1). The growth behavior of h-BN layers on and under Ni was also confirmed using a different precursor, borazine ($(BN)_3H_6$) (see the Supporting Information, Figures S2 and S3).

It has previously been suggested that h-BN layers are grown by the recrystallization of polymeric BN-rings following the adsorption of cyclic-BN on the metal surface.[10,16] In addition, N atoms are nearly insoluble in most transition metals, even at very high temperatures near 1000 °C, unlike highly soluble B atoms.[14,15] Thus, it has been assumed that h-BN formation is impossible at interfaces through metal. However, our results contradict these previous reports.

To understand the h-BN growth behavior at both the top and bottom sides of metals, we simulated the formation energies of h-BN layers and the reaction energies of BN precursors on and under the surfaces of two representative metal catalysts, Ni and Cu. The structural stability of h-BN layers on top of metal/SiO_2 and at the interface between the metal and SiO_2 was compared. These calculations showed that the h-BN layer at the interface between Ni and SiO_2 is more stable than the layer on top of the Ni surface by 0.85 eV, whereas the formation of the h-BN layer on top of the Cu surface is more stable than at the Cu/SiO_2 interface (Figure 2) by 3.68 eV (see Figure S4, Supporting Information).

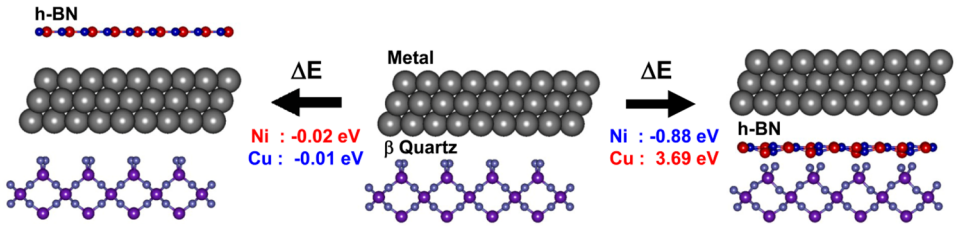

Figure 2. Calculations of structural stability of h-BN layers on top of metal/SiO_2 and at the interface between the metal and SiO_2. Blue, red, violet, and gray spheres visualize N, B, SiO_2, and metal atoms, respectively.

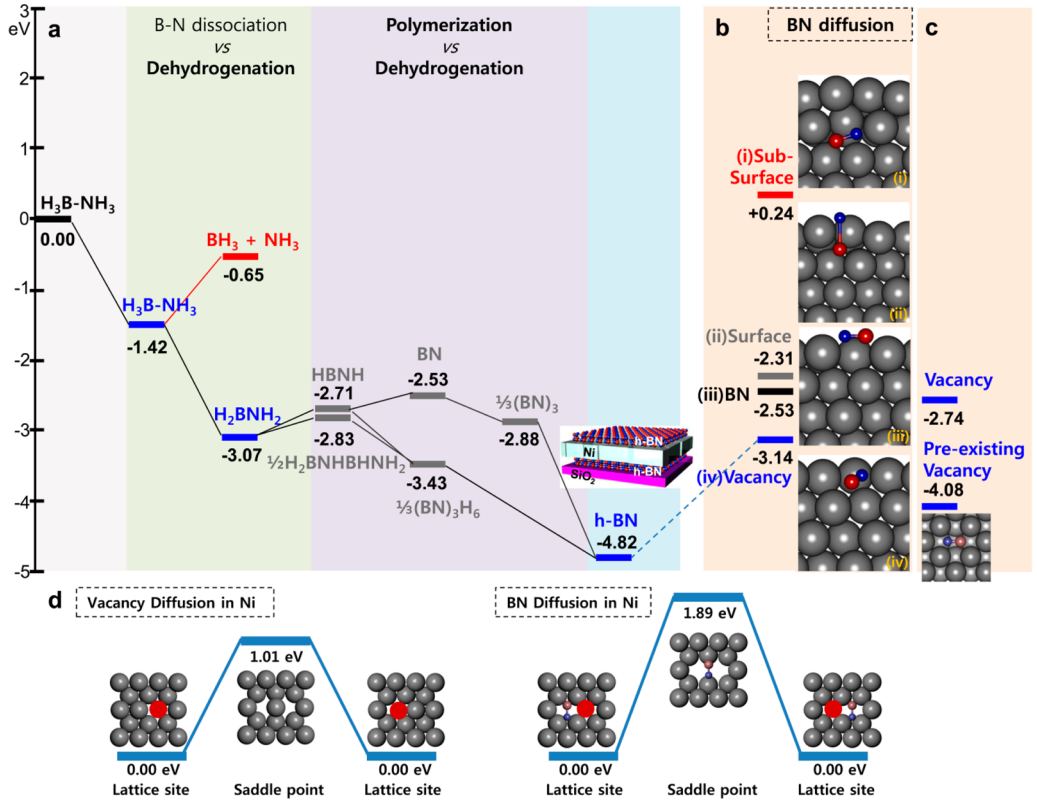

Figure 3. Reaction energy diagram for h-BN layer growth on and under the Ni metal. (a) Reaction coordination *vs* reaction energy for h-BN growth using AB. Blue line is a stable reaction path and red line is opposition. Gray line is energetically compatible. (b) Surface reaction energy of B−N molecule for diffusion. (c) Stability of B−N molecule in interstitial and vacancies in bulk Ni. (d) Diffusion barrier of Ni vacancy (left) and Ni vacancy mediated B−N molecule (right). Bulk Ni cut to (110) orientation and red circles are vacancy sites.

These results imply that h-BN formation at the interface is favorable for Ni but not for Cu.

To further clarify h-BN growth behavior at the interface, the reaction energies for the individual growth steps at the atomic scale were investigated. Figure 3a shows the reaction diagram of the AB precursor on Ni for h-BN formation. First, this diagram shows that dehydrogenation of H_3B-NH_3 occurs on the Ni surface, as this reaction is more favorable than B−N bond dissociation. Then, it shows that the dehydrogenation energy of H_2B-NH_2 is similar to the polymerization energy of H_2B-NH_2, indicating competition between these two processes. Finally, h-BN formation is energetically favorable and is achieved from cyclic BN ($^1/_3((BN)_3H_6)$) on the Ni surface. Collectively, these results reflect in the previous experimental reports.[10,16]

Interestingly, the formation of the B−N molecule by dehydrogenation on Ni was observed to be energetically stable, and its diffusion was explored for the proposed metal atomic vacancy-assisted interfacial growth. For this investigation, two well-known interstitial and substitutional diffusion mechanisms were considered.[23] For the interstitial diffusion mechanism, the stability of the B−N molecule was calculated for the movement of B−N molecules from the top of Ni to the subsurface. First, as B−N molecules are adsorbed onto the surface of Ni, only diffusion of B atoms is favorable. Due to the low solubility of N in Ni, N atoms are excluded from the surface, leading to elongation of the bond length from 1.39 to2.30 Å (Figure 3b (ii)). Then, when the B−N molecule is assumed to be included interstitially as a molecule, its incorporation

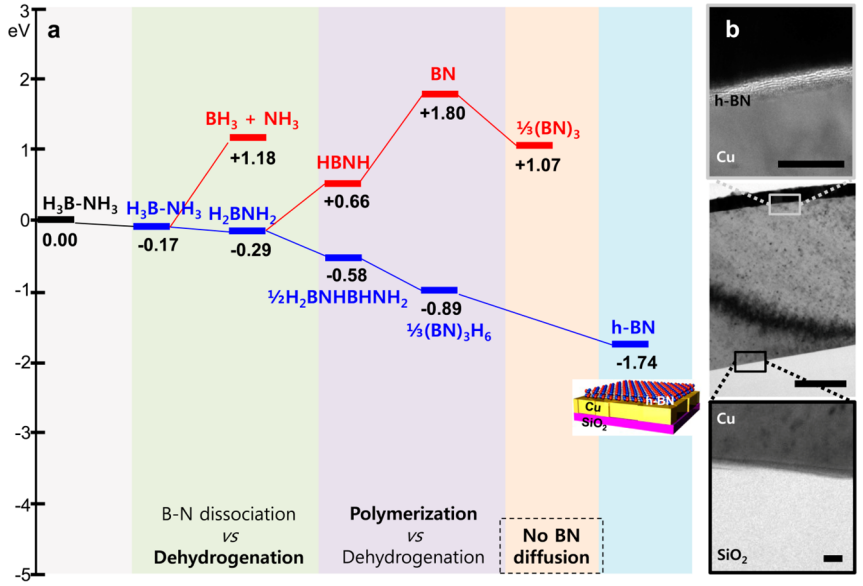

Figure 4. Reaction energy diagram for h-BN layer growth on Cu metal. (a) Reaction coordination *vs* reaction energy for h-BN growth. Blue line is a stable reaction path and red line is opposition. (b) HR-TEM images of grown h-BN layer on top of the Cu/SiO_2/Si substrate in experiment. Scales bars, 10 nm (top), 200 nm (middle) and 20 nm (bottom).

is energetically unstable (Figure 3b (i)). On the other hand, occupation of the B−N molecule in a surface vacancy is energetically favorable (Figure 3b (iv)) compared to adsorption of the B−N molecule onto the surface (Figure 3b (iii)). Furthermore, pre-existing Ni vacancies in the bulk can provide more stable sites than surface vacancies and allow for the diffusion of B−N molecules (Figure 3c bowwom).

To understand diffusion kinetics of B−N molecule in Ni, we simulated barrier heights for Ni vacancy diffusion and Ni vacancy mediated B−N molecule diffusion. We created vacancy from one of the nearest neighboring sites and simulated the diffusion barrier placing Ni and B−N molecule in the middle of the original position and the vacancy due to the symmetry of the lattice, as shown in Figure 3d. The energy barrier of Ni vacancy diffusion agrees well with previous work.[24] In addition, the diffusion barrier of B−N molecules placed on pre-existing vacancy in Ni (the most stable state, Figure 3C) is comparable to self-diffusion barrier heights of transition metals.[25] Thus, it is concluded that B−N molecules can diffuse into Ni through Ni atomic vacancies, which are abundant near grain boundaries, and then form h-BN layers at the interface, as shown in Figure 1a.

Notably, the h-BN growth behavior on Cu is completely different from that on Ni (Figure 4a). The reaction energy of each step on Cu is generally less stable than that on Ni. Furthermore, the formation of B−N molecules by dehydrogenation is energetically less favorable on Cu than on Ni. This result suggests that the formation of h-BN layers at the interface between Cu and SiO_2 is not favorable, as displayed in Figure 2, and agrees with the experimental result showing no h-BN growth at the Cu/SiO_2 interface (Figure 4b). Therefore, these results demonstrate that h-BN growth at the interface is strongly related to the formation of the B−N molecule and to its stability on the metal surface.

To further clarify the role of B−N molecular diffusion on the formation of h-BN at the Ni/SiO_2 interface, h-BN formation was investigated using a solid AB precursor at varying concentrations. A solid rather than gas precursor was chosen to avoid the penetration possibility through edge of substrate to the interface between the metal layer and SiO_2. Figure 5a shows a schematic illustration of h-BN formation on both sides of Ni by a thermal treatment using a solid precursor. AB precursors are converted into a polymeric −[NH═BN]$_n$− species above 130 °C, and the polymers are maintained as a solid near 1200 °C.[16] Briefly, the AB precursor was dissolved in 1 mL tetrahydrofuran (THF) at 20, 30, and 50 mg/mL and then spin-coated onto Ni (300 nm thickness)/SiO_2 substrates. The metal with a solid precursor was then preheated near 120 °C for 30 min to uniformly spread the precursor on the metal surface (see the Supporting Information Figure S6).

The h-BN layer formed by the solid precursor was grown not only on top of the Ni surface but also at the interface, indicating similar growth behavior compared to the gas precursor (Figure 1). HR-TEM images show that the h-BN layer thickness on top of the Ni surface and at the interface increased linearly with the precursor concentration (see Figure 5b−d and Figure S7, Supporting Information). Furthermore, a hexagonal crystalline structure was observed for both h-BN layers according to the FFT patterns (inset of Figure 5d). In the case of the top layer, all of the TEM images show amorphous BN phases on the crystalline h-BN layer (away from the metal surface) due to their formation

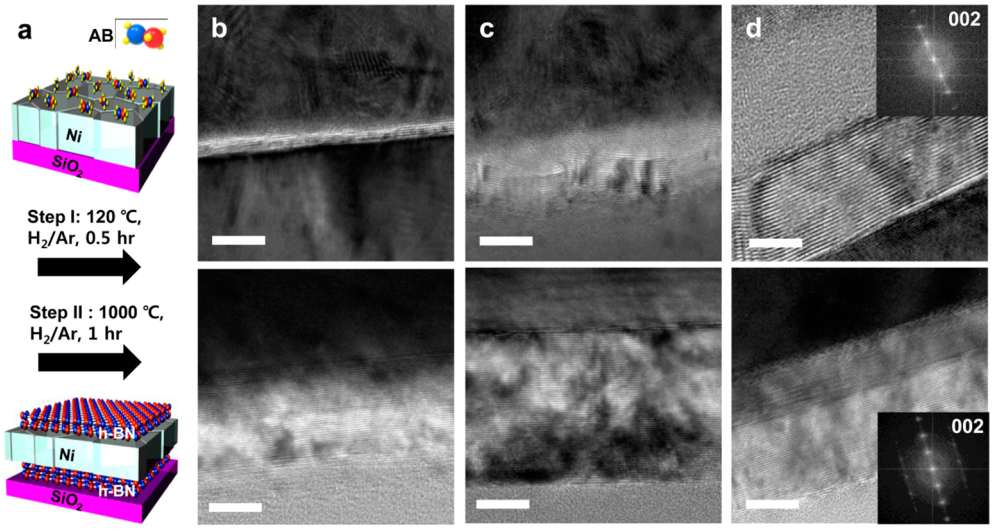

Figure 5. Characterization of CVD grown h-BN layers using a solid AB precursor. (a) Schematic illustration of h-BN formation on both sides of Ni by a thermal treatment using a solid precursor. Blue, red, and small yellow spheres visualize N, B, and H atoms, respectively. (b–d) HR-TEM images of h-BN layer grown by varying concentration of solid precursor: (b) 20 mg, (c) 30 mg, and (d) 50 mg in THF. Top row is top-layer and bottom row is interface-layer after thermal treatment. The corresponding FFT patterns were shown in inset of (d). Scale bar, 5 nm.

with less benefit from the metal (Figure 5b–d upside). In contrast, a pure crystalline h-BN structure is observed at the interface because B–N molecules diffused through the metal and continuously interacted with the metal during the formation of a new h-BN layer between preformed h-BN and Ni (Figure 5b–d downside). The thickness of the interfacial layer by the solid precursor is greater than that of the top layer, which is in contrast to the gas precursor results shown in Figure 1a. This result provides clear evidence of B–N molecular diffusion in the metal. Furthermore, it suggests that predeposited solid AB precursor has a greater chance to diffuse in the metal, while presynthesized h-BN layers in the gas precursor system could have prevented the precursor reaction with metal. Large-sized, continuous h-BN layers were obtained from both sides of the metal after conventional transfer methods (see Figure S8, Supporting Information).[11]

CONCLUSION

We have shown that h-BN layers can be formed on top of Ni by a surface reaction of precursors and also at the interface between Ni and an underlying oxide substrate by B–N molecular diffusion. The h-BN layer at the interface between Ni and SiO_2 is relatively stable, whereas the layer on top of Cu/SiO_2 is favorable. Eventually, the formation and stability of B–N molecules on Ni metal can provide an opportunity for interfacial growth by metal atomic vacancy-assisted B–N molecular diffusion. Furthermore, h-BN formation at the interface by the solid precursor clearly proved the B–N molecular diffusion. The solid precursor also provides a means for controlling the h-BN layer thickness on the oxide substrate with clean structure. This method could be useful for directing h-BN growth on substrates that are to be utilized in 2D electronics without requiring any transfer process that could generate defects.

METHODS

Growth of Hexagonal Boron Nitride (h-BN). Ni (300 nm)-deposited SiO_2/Si substrates were placed in an ambient pressure CVD chamber and gradually heated up to 1000 °C for 2 h 30 min in a mixed Ar/H_2 (80:20 vol %) flow with a flow rate of 100 sccm. Then, the main growth was carried out in a mixed Ar/H_2 gas flow of 75 sccm for 30 min at 1000 °C with ammonia borane (AB, $H_3B–NH_3$) as the precursor material. AB was sublimated at 110–130 °C using a subheating chamber with a N_2 gas flow of 25 sccm. Finally, after the main growth, the chamber was cooled to 180 °C with a mixed Ar/H_2 gas flow at a flow rate of 100 sccm for 4 h.

Characterization of Both h-BN Layers on and under Metal. Cross-sectional high-resolution transmission electron microscopy (HR-TEM) (Tecnai Titan 80-300, FEO Co) provided further insight into the existence of the h-BN layer at the interface between the Ni catalyst and SiO_2/Si substrates after the growth process. HR-TEM was also used to investigate the film crystallinity and the diffraction pattern by the fast Fourier transform (FFT) method. The interlayer distance of the h-BN layer was obtained from the intensity profile of the lines at the edges. The structural quality was characterized by electron energy-loss spectroscopy (EELS) measurements. Raman spectroscopy (RM-1000 Invia, 514 nm, Ar^+ ion laser, Renishaw) and X-ray photoelectron spectroscopy (XPS) (QUANTUM 2000, Physical Electronics) were also used to characterize the h-BN layer.

General Methods for Computational Modeling. The formation energies of the h-BN layer and the reaction energies of the BN precursors were determined using first-principles calculations performed using the density functional theory (DFT)-based pseudopotential method.[19] The DFT simulations were performed using the Vienna *ab initio* simulation package with the Perdew–Burke–Ernzerhof (PBE) exchange-correlation functional and the projector augmented-wave pseudopotential.[26,27]

Formation Energy of h-BN Layer on and under Metal. Stack structures consisting of a single surface unit cell of β-quartz, 2×2 surface unit cells of metal catalyst (Ni or Cu), and 2×2 unit cells of h-BN were used. The lattice mismatch between the stack structures was less than 3% (see Table S1, Supporting Information). The β-quartz lattice constant was used as the reference for all of the simulations. β-Quartz has five Si layers, with the bottom oxygen layers terminating in hydrogen, while the metals used have three atomic layers. During relaxation, the bottom hydrogen layer, the oxygen layers, and the bottommost Si layers were fixed in their bulk positions. A $6 \times 6 \times 1$ k-point sampling was adopted.

Reaction Energy of BN Precursor. Slab structures with Ni (111) and Cu (111) orientations were used, as these are the most stable surface orientations in face-centered cubic (fcc) structures. For the small molecule simulations, such as those related to H_3BNH_3 and its dehydrated structures, the slabs used were 3×3 surface unit cells with four atomic layers. For larger molecules, such as $B_3N_3H_6$, the slabs were 5×5 surface unit cells to keep a similar B−N density on metal surfaces. All atoms were relaxed, except those in the bottom two layers, which were kept at their bulk positions. A $4 \times 4 \times 1$ k-point sampling was adopted. For the surface and interface simulations, vacuum spaces more than 15 Å in size were inserted to prevent interactions between repeating images. For the bulk simulations, $3 \times 3 \times 3$ fcc unit cells were used with a $3 \times 3 \times 3$ k-point sampling. The reaction energies were calculated with respect to the metal surface and the AB precursor for the surface reactions and with respect to the metal bulk and the AB precursor for the bulk simulations. It was assumed that all of the hydrogen atoms that detached from the AB precursor during the reactions were desorbed in the form of hydrogen molecules. A cutoff energy of 36.75 Ry was used.

Conflict of Interest: The authors declare no competing financial interest.

Acknowledgment. S.-W.K. acknowledges financial support from the Basic Research Program (2012R1A2A1A01002787 and 2009-0083540) of the National Research Foundation of Korea (NRF) grant funded by the Ministry of Science, ICT & Future Planning (MSIP).

Supporting Information Available: In depth description of the h-BN growth on and under Ni according to precursor type, AB precursor (Figure S1), and borazine (Figure S2) and analysis of their top layer (Figures S3). Computational model for h-BN formation (Figure S4) and reaction diagram for h-BN growth (Figure S5) at the interface between metal catalyst and oxide substrate. h-BN growth on and under Ni using solid AB precursor results (Figure S6−S8). This material is available free of charge *via* the Internet at http://pubs.acs.org.

REFERENCES AND NOTES

1. Kim, K.; Choi, J.-Y.; Kim, T.; Cho, S.-H.; Chung, H. J. A Role for Graphene in Silicon-Based Semiconductor Devices. *Nature* **2011**, *479*, 338–344.
2. Yang, H.; Heo, J.; Park, S.; Song, H. J.; Seo, D. H.; Byun, K. E.; Kim, P.; Yoo, I.; Chung, H. J.; Kim, K. Graphene Barristor, a Triode Device with a Gate-Controlled Schottky Barrier. *Science* **2012**, *336*, 1140–1143.
3. Britnell, L.; Gorbachev, R. V.; Jalil, R.; Belle, B. D.; Schedin, F.; Mishchenko, A.; Georgiou, T.; Katsnelson, M. I.; Eaves, L.; Morozov, S. V.; *et al.* Field-Effect Tunneling Transistor Based on Vertical Graphene Heterostructures. *Science* **2012**, *335*, 947–950.
4. Yu, W. J.; Li, Z.; Zhou, H. L.; Chen, Y.; Wang, Y.; Huang, Y.; Duan, X. F. Vertically Stacked Multi-Heterostructures of Layered Materials for Logic Transistors and Complementary Inverters. *Nat. Mater.* **2013**, *12*, 246–252.
5. Georgiou, T.; Jalil, R.; Belle, B. D.; Britnell, L.; Gorbachev, R. V.; Morozov, S. V.; Kim, Y. J.; Gholinia, A.; Haigh, S. J.; Makarovsky, O.; *et al.* Vertical Field-Effect Transistor Based on Graphene−WS_2 Heterostructures for Flexible and Transparent Electronics. *Nat. Nanotechnol.* **2013**, *8*, 100–103.
6. Kim, K. S.; Zhao, Y.; Jang, H.; Lee, S. Y.; Kim, J. M.; Kim, K. S.; Ahn, J. H.; Kim, P.; Choi, J. Y.; Hong, B. H. Large-Scale Pattern Growth of Graphene Films for Stretchable Transparent Electrodes. *Nature* **2009**, *457*, 706–710.
7. Li, X. S.; Cai, W. W.; An, J. H.; Kim, S.; Nah, J.; Yang, D. X.; Piner, R.; Velamakanni, A.; Jung, I.; Tutuc, E.; *et al.* Large-Area Synthesis of High-Quality and Uniform Graphene Films on Copper Foils. *Science* **2009**, *324*, 1312–1314.
8. Lee, Y.-H.; Zhang, X. Q.; Zhang, W. J.; Chang, M. T.; Lin, C. T.; Chang, K. D.; Yu, Y. C.; Wang, J. T. W.; Chang, C. S.; Li, L. J.; *et al.* Synthesis of Large-Area MoS_2 Atomic Layers with Chemical Vapor Deposition. *Adv. Mater.* **2012**, *24*, 2320–2325.
9. Song, Li.; Ci, L.; Lu, H.; Sorokin, P. B.; Jin, C.; Ni, j.; Kvashnin, A. G.; Kvashnin, D. G.; Lou, J.; Yakoboson, B. I.; *et al.* Large Scale Growth and Characterization of Atomic Hexagonal Boron Nitride Layers. *Nano Lett.* **2010**, *10*, 3209–3215.
10. Shi, Y.; Hamsen, C.; Jia, X.; Kim, K. K.; Reina, A.; Hofmann, M.; Hsu, A. L.; Zhang, K.; Li, H.; Juang, Z.-Y.; Dresselhaus, M. S.; *et al.* Synthesis of Few-Layer Hexagonal Boron Nitride Thin Film by Chemical Vapor Deposition. *Nano Lett.* **2010**, *10*, 4134–4139.
11. Lee, K. H.; Shin, H.-J.; Lee, J.; Lee, I.-Y.; Kim, G.-H.; Choi, J.-Y.; Kim, S.-W. Large-Scale Synthesis of High-Quality Hexagonal Boron Nitride Nanosheets for Large-Area Graphene Dlectronics. *Nano Lett.* **2012**, *12*, 714–718.
12. Brenner, D. W. Empirical Potential for Hydrocarbons for Use in Simulating the Chemical Vapor Deposition of Diamond Films. *Phys. Rev. B* **1990**, *42*, 9458.
13. Wagner, R. S.; Ellis, W. C. Vapor-Liquid-Solid Mechanism of Single Crystal Growth. *Appl. Phys. Lett.* **1964**, *4*, 89–90.
14. Chakrabarti, D. J.; Laughlin, D. E. The B-Cu (Boron-Copper) System. *Alloy Phase Diagrams* **1982**, *3*, 45–48.
15. Springer Materials. The Landolt−Börnstein database (http://www.springermaterials.com). DOI: 10.1007/10086090_1091.
16. Samuel, F.; Richard, K.; Carl, M.; Trent, M.; William, S. W.; Cecil, K.; Steven, L. S. Pyrolytic Decomposition of Ammonia Borane to Boron Nitride. *Inorg. Chem.* **2011**, *50*, 783–792.
17. Suzuki, S.; Pallares, R. M.; Hibino, H. Growth of Atomically Thin Hexagonal Boron Nitride Films by Diffusion through a Metal Film and Precipitation. *J. Phys. D: Appl. Phys.* **2012**, *45*, 385304.
18. Suzuki, S.; Pallares, R. M.; Orofeo, C. M.; Hibino, H. Boron Nitride Growth on Metal Foil using Solid Sources. *J. Vac. Sci. Technol.* **2013**, *31*, 041804.
19. Payne, M. C.; Teter, M. P.; Allan, D. C.; Arias, T. A.; Joannopoulos, J. D.Iterative Minimization Techniques for *ab initio* Total-Energy Calculations: Molecular Dynamics and Conjugate Gradient. *Rev. Mod. Phys.* **1992**, *64*, 1054.
20. Hod, O. *J. Chem.* Graphite and Hexagonal Boron-Nitride have the Same Interlayer Distance. Why? *Theory Comput.* **2012**, *8*, 1360–1369.
21. Stephan, O.; Ajayan, P. M.; Colliex, C.; Redlich, Ph.; Lambert, J. M.; Bernier, P.; Lefin, P. Doping Graphitic and Carbon Nanotube Structures with Boron and Nitrogen. *Science* **1994**, *266*, 1683–1685.
22. Moulder, J. F.; Stickle, W. F.; Sobol, P. E.; Bomben, K. D. *Handbook of X-ray Photoelectron Spectroscopy: A Reference Book of Standard Data for Use in X-ray Photoelectron Spectroscopy*; Chastain, J., Eds; Physical Electronics: Minneapolis, 1992; pp 1−261.
23. Balluffi, R. W.; Mehl, R. F. Grain Boundary Diffusion Mechanisms in Metals. *Metall. Mater. Trans. B* **1982**, *13*, 527–553.
24. Janotti, A.; Krčmar, M.; Fu, C. L.; Reed, R. C. Solute Diffusion in Metals: Larger Atoms Can Move Faster. *Phys. Rev. Lett.* **2004**, *92*, 085901.
25. Krčmar, M.; Fu, C. L.; Janotti, A.; Reed, R. C. Diffusion Rates of 3d Transition Metal Solutes in Nikel by First Principles Calculations. *Acta Mater.* **2005**, *53*, 2369–2376.
26. Kresse, G.; Hafner, J. *Ab Initio* Molecular Dynamics for Liquid Metals. *Phys. Rev. B* **1993**, *47*, 558.
27. Blochl, P. E. Projector Augmented-Wave Method. *Phys. Rec. B* **1994**, *50*, 17953.